

# Adversarially-learned Inference via an Ensemble of Discrete Undirected Graphical Models

Adarsh K. Jeewajee  
MIT CSAIL  
jaks19@mit.edu

Leslie P. Kaelbling  
MIT CSAIL  
lpk@csail.mit.edu

## Abstract

Undirected graphical models are compact representations of joint probability distributions over random variables. To solve inference tasks of interest, graphical models of arbitrary topology can be trained using empirical risk minimization. However, to solve inference tasks that were not seen during training, these models (EGMs) often need to be re-trained. Instead, we propose an inference-agnostic adversarial training framework which produces an infinitely-large ensemble of graphical models (AGMs). The ensemble is optimized to generate data within the GAN framework, and inference is performed using a finite subset of these models. AGMs perform comparably with EGMs on inference tasks that the latter were specifically optimized for. Most importantly, AGMs show significantly better generalization to unseen inference tasks compared to EGMs, as well as deep neural architectures like GibbsNet and VAEAC which allow arbitrary conditioning. Finally, AGMs allow fast data sampling, competitive with Gibbs sampling from EGMs.

## 1 Introduction

Probabilistic graphical models [Koller and Friedman, 2009, Murphy, 2012] are compact representations of joint probability distributions. We focus on *discrete pairwise undirected* graphical models, which represent the independence structure between pairs of random variables. Algorithms such as belief propagation allow for inference on these graphical models, with arbitrary choices of observed, query and hidden variables. When the graph topology is loopy, or when the structure is mis-specified, inference through belief propagation is approximate [Murphy et al., 2013].

A purely generative way to train such a model is to maximize the likelihood of training data (ML), under the probability distribution induced by the model. However, evaluating the gradient of this objective involves computing marginal probability distributions over the random variables. As these marginals are approximate in loopy graphs, the applicability of likelihood-trained models to discriminative tasks is diminished [Kulesza and Pereira, 2008]. In these tasks, the model is called upon to answer queries expressed compactly as  $(X_{\mathcal{E}} = x_{\mathcal{E}}, X_{\mathcal{Q}}, X_{\mathcal{H}})$ , where from a data point  $(x_1, \dots, x_N)$  sampled from a certain data distribution  $\mathbb{P}$ , we observe the values of a subset  $\mathcal{E}$  of the indices, and have to predict the values at indices in  $\mathcal{Q}$  from a discrete set  $\mathcal{X}$ , with the possibility of some hidden variable indices  $\mathcal{H}$  which have to be marginalized over:

$$\arg \max_{x \in \mathcal{X}} \mathbb{P}(X_i = x | X_{\mathcal{E}} = x_{\mathcal{E}}), \forall i \in \mathcal{Q}. \quad (1)$$

A distribution over queries of this form will be referred to as an inference task. If the distribution over queries that the model will be called upon to answer is known a priori, then the model’s performance can be improved by shaping the query distribution used at parameter estimation time, accordingly.

In degenerate tasks,  $\mathcal{E}$ ,  $\mathcal{Q}$  and  $\mathcal{H}$  are fixed across queries. When this is the case *and*  $\mathcal{H}$  is empty, we could use a Bayesian feed-forward neural network [Husmeier and Taylor, 1999] to model the

distribution in (1) and train it by backpropagation. The *empirical risk minimization of graphical models* (EGM) framework of Stoyanov et al. [2011] and Domke [2013] generalizes this gradient-descent-based parameter estimation idea to graphical models. Their framework allows retaining any given graphical model structure, and back-propagating through a differentiable inference procedure to obtain model parameters that facilitate the query-evaluation problem. EGM allows solving the most general form of problems expressed as (1), where  $\mathcal{E}$ ,  $\mathcal{Q}$  and  $\mathcal{H}$  are allowed to vary. Information about this query distribution is used at training time to *sample* choices of evidence, query and hidden variable *indices* ( $\mathcal{E}$ ,  $\mathcal{Q}$ ,  $\mathcal{H}$ ), as well the *observed values*  $x_{\mathcal{E}}$  across data points. The whole imperfect system is then trained end-to-end through gradient propagation [Domke, 2010]. This approach improves the inference accuracy on this specific query distribution, by orders of magnitude compared to the ML approach. One significant drawback of the EGM approach is that the training procedure is tailored to one specific inference task. To solve a different inference task, the model often has to be completely re-trained (as we see in section 4).

Instead, we would like to learn discrete undirected graphical models which generalize over different or multi-modal inference tasks. Our *adversarially trained graphical model* (AGM) strategy is built on the GAN framework [Goodfellow et al., 2014]. It allows us to formulate a learning objective for our graphical models, aimed purely at optimizing the generation of samples from the model. No information about inference tasks is baked into this learning approach. Our only assumption during training is that the training and testing *data points* come from the same underlying distribution. Although our undirected graphical models need to be paired to a neural learner for the adversarial training, they are eventually detached from the learner, with an ensemble of parameterizations. When using one of the parameterizations, our graphical model is indistinguishable from one that was trained using alternative methods. We propose a mechanism for performing inference with the whole ensemble, which provides the desired generalization properties across inference tasks, improving over EGM performance. Our learning approach is essentially generative, but the ensemble of models increases the expressive power of the final model, making up for approximations in inference and model mis-specification which affected the ML approach discussed above.

In the next sections, we discuss related work (2) and introduce our adversarial training framework (3) for undirected graphical models. Our first experiment (4.1), shows that although undirected graphical models with empirical risk minimization (EGMs) are trained specifically for certain inference tasks, our adversarially-trained graphical models (AGMs) can perform comparatively, despite having never seen those tasks prior to training. The second experiment (4.2) is our main experiment which showcases the generalization capabilities of AGMs across unseen inference tasks on images. We also compare AGMs against state-of-the-art neural models GibbsNet and VAEAC which, like AGMs, were designed for arbitrary conditioning. In the last experiment (4.3), we show that the combination of AGMs and their neural learner provide a viable alternative for sampling from joint probability distributions in one shot, compared to Gibbs samplers defined on EGMs.

## 2 Related work

Our work combines *discrete, undirected* graphical models with the *GAN* framework for training. The graphical model is applied in *data space*, with the *belief propagation* algorithm used for *inference*, over an *ensemble of parameterizations*.

Combining an ensemble of models has been explored in classification [Bahler and Navarro, 2000] and unsupervised learning [Baruque, 2010]. Combined models may each be optimized for a piece of the problem space [Jacobs et al., 1991] or may be competing on the same problem [Freund and Schapire, 1999]. Linear and log-linear ensemble combinations like ours have been analyzed by Fumera and Roli [2005] and the closest work which uses the ensemble approach, by Antonucci et al. [2013], combines Bayesian networks for classification. Furthermore, our ensemble is obtained through the idea of one module learning to output the parameters of another module, which has its roots in meta learning. In Bertinetto et al. [2016] and Munkhdalai and Yu [2017], one neural network learns to assign weights to another network with and without the help of memory, respectively.

Using GANs to generate data from *discrete* distributions is an active area of research, including work of Fathony and Goela [2018], Dong and Yang [2018], and Camino et al. [2018], with applications in health [Choi et al., 2017] and quantum physics [Situ et al., 2018]. Undirected graphical models have been embedded into neural pipelines before. For instance, Zheng et al. [2015] use them as

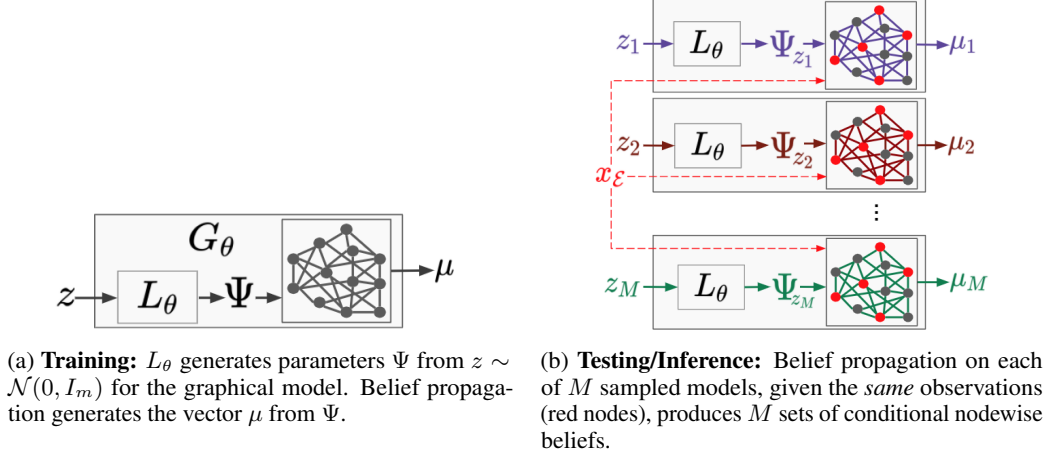


Figure 1: Our framework, during training (left) and during testing/inference (right).

RNNs, Ammar et al. [2014] and Johnson et al. [2016] use them in the neural autoencoder framework, Kuleshov and Ermon [2017] use them in neural variational inference pipelines, and Tompson et al. [2014] combine them with CNNs.

Other works use graph neural networks [Battaglia et al., 2018], but with some connection to classical undirected graphical models. For example, some works learn variants of, or improve on, message passing [Liu and Poulin, 2019, Satorras and Welling, 2020, Gilmer et al., 2017, Satorras et al., 2019]. Other works combine classical graphical models and graph neural networks with one another [Qu et al., 2019], while some use neural networks to replace classical graphical model inference entirely [Yoon et al., 2018, Zhang et al., 2019].

Some previous works combine graphical models with neural modules, but for *structured* inference. They assume a fixed set of input and output variables, solving problems such as image tagging [Chen et al., 2015, Tu and Gimpel, 2018] and classification [Tu and Gimpel, 2018]. These methods do *not* solve problems with arbitrary conditioning. On the other hand, *purely neural* models such as those developed in Ivanov et al. [2019], Douglas et al. [2017] and Belghazi et al. [2019] do tackle arbitrary conditioning problems formulated as (1). Being purely neural, the variational autoencoder (VAEC) approach of Ivanov et al. [2019], however, requires masks defined over random variables during training to match conditioning patterns expected in test inference tasks, while we are *completely* agnostic to inference during training. We compare of our method against VAEC in our experiments.

Among the work closest to ours, Fathony et al. [2018] learn *tractable* graphical models using *exact inference* through adversarial objectives. Chongxuan et al. [2018] and Karaletsos [2016] use graphical models in adversarial training pipelines, but to model posterior distributions. GANs have been used with graphs for high-dimensional representation learning [Wang et al., 2017], structure learning [Bojchevski et al., 2018] and classification [Zhong and Li, 2018]. Other relevant GAN works focus on inference in the data space without the undirected graphical structure. For example the conditional GAN [Mirza and Osindero, 2014] and its variants [Xu et al., 2019] allow inference, but conditioned on variables specified during training. [Donahue et al., 2016] and [Dumoulin et al., 2017] introduced the idea of learning the reverse mapping from data space back to latent space in GANs. GibbsNet [Lamb et al., 2017] is the closest model to us in terms of allowing arbitrary conditioning and being trained adversarially, although it is *not* a probabilistic model. The inference process of GibbsNet is iterative as it transitions from data space to latent space and back, stochastically several times, clamping observed values in the process. Our inference mechanism does not operate in a latent space, but is also iterative due to the belief propagation algorithm. Each model in our learned ensemble has significantly less parameters than GibbsNet, and we compare the performance of our method against GibbsNet in our experiments.

### 3 Method

**Preliminaries** We aim to learn the parameters for pairwise discrete undirected graphical models, adversarially. These models are structured as graphs  $G(V, E)$ , with each node in their node set  $V$

representing one variable in the joint probability distribution being modeled. The distribution is over variables  $X_1^N := (X_1, \dots, X_N)$ . For simplicity, we assume that all random variables can take on values from the same discrete set  $\mathcal{X}$ .

A graphical model carries a parameter vector  $\Psi$ . On each edge  $(i, j) \in E$ , there is one scalar  $\psi_{i,j}$  for every pair of values  $(x_i, x_j)$  that the pair of connected random variables can admit. Therefore every edge carries  $|\mathcal{X}|^2$  parameters, and in all, the graphical model  $G(V, E)$  carries  $k = |E||\mathcal{X}|^2$  total parameters, all contained in the vector  $\Psi \in \mathbb{R}^k$ .

Through its parameter set  $\Psi$ , the model summarizes the joint probability distribution over the random variables up to a normalization constant  $\mathcal{Z}$  as:

$$q_{X_1^N}(x_1^N; \Psi) = \frac{1}{\mathcal{Z}} \prod_{(i,j) \in E} \psi_{i,j}(x_i, x_j). \quad (2)$$

Instead of incrementally updating *one* set of parameters  $\Psi$  to train a graphical model  $G(V, E)$ , our method trains an uncountably infinite *ensemble* of graphical model parameters, adversarially. By learning an ensemble, we make up for the fact that our base graphical model structure may be mis-specified and may not be able to represent the true joint probability distribution over random variables of interest, and that inference on graphical models of arbitrary topologies is approximate. In our framework, our model admits a random vector  $z \in \mathbb{R}^m$  sampled from a standard multivariate Gaussian distribution as well as a deterministic transformation  $L_\theta$ , from  $z$  to a graphical model parameter vector  $\Psi_z = L_\theta(z) \in \mathbb{R}^k$ , where  $\theta$  is to be trained. Under our framework, the overall effective joint distribution over random variables  $X_1^N$  can be summarized as

$$p_{X_1^N}(x_1^N) = \int_{z \in \mathbb{R}^m} p_Z(z) p_{X_1^N|Z}(x_1^N|z) dz = \int_{z \in \mathbb{R}^m} p_Z(z) q_{X_1^N}(x_1^N; L_\theta(z)) dz \quad (3)$$

Through adversarial training, we will learn to map random vectors  $z \in \mathbb{R}^m$  to data samples. The only learnable component of this mapping is the transformation of  $z \in \mathbb{R}^m$  to  $\Psi_z \in \mathbb{R}^k$  through  $L_\theta$ . Given  $\Psi_z$ , the joint distribution  $q_{X_1^N}(x_1^N; \Psi_z)$  is given in (2) and since the goal of adversarial training is to produce high-quality samples which are indistinguishable from real data through the lens of some discriminator, the training process is essentially priming each  $\Psi_z = L_\theta(z)$  to specialize on a niche region of the domain of the true data distribution. From the point of view of Jacobs et al. [1991], we will have learnt ‘local experts’  $\Psi_z$ , each specializing to a subset of the training distribution. The entire co-domain of  $L_\theta$  is our ensemble of graphical model parameterizations.

Finally, we will use an inference procedure throughout our exposition. Computing exact marginal probabilities using (2) is intractable. Hence, whenever we are given a graphical model structure, one parameter vector  $\Psi$  and some observations  $x_\mathcal{E}$ , we carry out a fixed number  $t$  of belief propagation iterations through the  $\text{inference}(x_\mathcal{E}, \Psi, t)$  procedure, to obtain one *approximate* marginal probability distribution  $\mu_i$ , conditioned on  $x_\mathcal{E}$ , for every  $i \in V$ . Note that the distributions  $\mu_i$  for  $i \in \mathcal{E}$  are degenerate distributions with all probability mass on the observed value of random variable  $X_i$ . In our work, we will use this inference procedure with  $\mathcal{E} = \emptyset$  and  $\mathcal{E} \neq \emptyset$ , during the learning and inference phases, respectively.

**Adversarial training** Our adversarial training framework follows Goodfellow et al. [2014]. The discriminator  $D_w$  is tasked with distinguishing between real and fake samples in data space. Our  $(L_\theta, G(V, E))$  pair constitutes our generator  $G_\theta$  as seen in figure 1a. Fake samples are produced by our generator  $G_\theta$ , which as is standard, maps a given vector  $z$  sampled from a standard multivariate Gaussian distribution, to samples  $\tilde{x}$ .

One layer of abstraction deeper, the generative process  $G_\theta$  is composed of  $L_\theta$  taking in random vector  $z \in \mathbb{R}^m$  as input, and outputting a vector  $v \in \mathbb{R}^k$ . The graphical model receives  $v$ , runs  $\text{inference}(x_\mathcal{E} = \emptyset, \Psi = v, t = t')$ , for a pre-determined  $t'$ , and outputs a set of marginal probability distributions  $\mu_i$  for  $i \in V$ . Note that the set  $\mathcal{E}$  of observed variables is empty, since our training procedure is inference-agnostic.

In summary, the graphical model extends the computational process which generated  $v$  from  $z$ , with the deterministic recurrent process of belief propagation on its structure  $E$ . Note that a one-to-one correspondence between entries of  $v$  and graphical model parameters  $\psi_{i,j}(x_i, x_j)$  has to be pre-determined for  $L_\theta$  and  $G(V, E)$  to interface with one another.

Instead of categorical sampling from the beliefs  $\mu_i$  to get a generated sample for the GAN training [Hjelm et al., 2017, Jang et al., 2017], we follow the WGAN-GP method of Gulrajani et al. [2017] for training our discrete GAN. In their formulation, the fake data point  $\tilde{x}$  is a concatenation of all the marginal probability distributions  $\mu_i$ , in some specific order. This means that true samples from the training data set have to be processed into a concatenation of the  $\mathcal{X}$ -dimensional one-hot encodings of the values they propose for every node, to meet the input specifications of the discriminator.

We optimize the WGAN-GP objective (4) with the gradient  $\nabla_{x'} \|D_w(x')\|_2$  penalized at points  $x' = \epsilon x + (1 - \epsilon)\tilde{x}$  which lie on the line between real samples  $x$  and fake samples  $\tilde{x}$ . This regularizer is a tractable 1-Lipschitz enforcer on the discriminator function, which stabilizes the WGAN-GP training procedure:

$$\min_w \max_{\theta} \mathbb{E}_{\tilde{x} \sim \mathbb{Q}} [D_w(\tilde{x})] - \mathbb{E}_{x \sim \mathbb{P}} [D_w(x)] + \lambda \mathbb{E}_{x' \sim \mathbb{P}'} \left[ (\nabla_{x'} \|D_w(x')\|_2 - 1)^2 \right]. \quad (4)$$

**Inference using the ensemble of graphical models** Out of the various ways to coordinate responses from our ensemble of graphical model parameters (see section 2), we choose the log-linear pooling method of [Antonucci et al., 2013], for its simplicity. Given a query of the form  $(X_{\mathcal{E}} = x_{\mathcal{E}}, X_{\mathcal{Q}}, X_{\mathcal{H}})$  as seen in (1), we call upon a finite subset of our infinite ensemble of graphical models. We randomly sample  $M$  random vectors  $z_1, \dots, z_M$  from the standard multivariate Gaussian distribution and map them to a collection of  $M$  parameter vectors  $(\Psi_1 = L_{\theta}(z_1), \dots, \Psi_M = L_{\theta}(z_M))$ .  $M$  sets of beliefs, for every node, are fetched through  $M$  parallel calls to the inference procedure: `inference`  $(x_{\mathcal{E}}, \Psi = L_{\theta}(z_j), t = t')$  for  $j = 1, \dots, M$ . The idea behind log-linear pooling is to aggregate the opinion of every model in this finite collection. Concretely, for every random variable  $X_i$ , its  $M$  obtained marginal distributions  $\mu_i(\cdot | x_{\mathcal{E}}; \Psi_j)$  for  $j = 1, \dots, M$  are aggregated as we show in (5):

$$\hat{x}_i = \arg \max_{x \in \mathcal{X}} \prod_{j=1}^M \mu_i(x | x_{\mathcal{E}}; \Psi_j)^{\frac{1}{M}}. \quad (5)$$

Obtaining marginal probability distributions through an ensemble of graphical models is reminiscent of the tree-reweighted belief propagation algorithm of Wainwright et al. [2002], which produces these marginals using *one* set of parameters, and by re-formulating the belief propagation procedure to encompass the entire *polytope of spanning tree structures* associated with a set of random variables. In our work we learn a *variety of parameterizations*, over *one* fixed arbitrary graph topology, to make up for inaccuracies in that topology as well as the approximate nature of our inference procedure. Combining both ideas to learn an ensemble of parameterizations defined over a collection of structures is an interesting direction for future work.

## 4 Experiments

For inference tasks of the type formulated in (1), we need to define strategies for creating queries of the form:  $(X_{\mathcal{E}} = x_{\mathcal{E}}, X_{\mathcal{Q}}, X_{\mathcal{H}})$ . To construct any query, we start by sampling one data point from a distribution (data set) of interest. We then choose which variables to reveal as observations and we keep the original values of the rest of the variables (query variables) as targets. An inference task is created by applying one of the following (possibly stochastic) patterns to sampled data points:

- (i) `fractional`( $f$ ): A fraction  $f$  of all variables is selected at random and turned into query variables, and the rest are revealed as evidence.
- (ii) `corrupt`( $c$ ): Every variable is independently switched, with probability  $c$ , to another value picked uniformly at random, from its discrete support. Then `fractional`(0.5) is applied to the data point to obtain the query as in (i).
- (iii) `window`( $w$ ): [Image only] The center square of width  $w$  pixels is hidden and those pixels become query variables, while the pixels around the square are revealed as evidence.
- (iv) `quadrant`( $q$ ): [Image only] One of the four quadrants of pixels is hidden, and those pixels become query variables. The other three quadrants are revealed as evidence.

Some instantiations of these schemes, with specific parameters, on image data, are shown in figure 2. We note that the train and test query creation policies do not have to match. In fact, the strength of

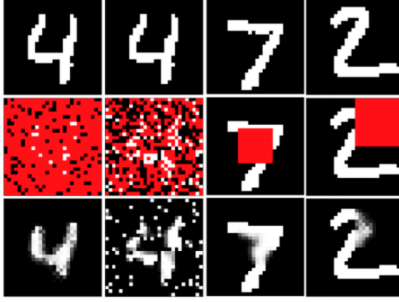


Figure 2: In columns 1 to 4, query-creation schemes are: `fractional(0.85)`, `corrupt(0.2)`, `window(10)` and `quadrant(1)`, respectively. Row 1: original data; row 2: data is converted to queries ( $X_{\mathcal{E}} = x_{\mathcal{E}}, X_{\mathcal{Q}}, X_{\mathcal{H}}$ ) (non-red pixels are observations  $x_{\mathcal{E}}$ , red pixels are variables  $X_{\mathcal{Q}}$  to be guessed); row 3: marginals produced by *one* AGM, where  $\mathbb{P}(\text{pixel} = 1)$  is plotted. Note that the dots apparent in row 3 column 2 are due to unchanged corrupted pixels which we count as observations.

Table 1: Data set information and accuracies from experiments I and III. Every value is *averaged over 5 repeats*, with an error bar smaller than  $\pm 0.5$ .

Name	Experiment I			Experiment III		
	EGM	AGM (ours)	EGM-AGM	AGM sampler	Gibbs sampler (burn=0)	Gibbs sampler (burn=10)
NLTCS	81.7	79.5	+2.2	81.2	77.7	79.8
Jester	70.6	65.7	+4.9	69.88	63.9	67.0
Netflix	66.0	63.9	+2.1	64.7	61.4	61.8
Accidents	83.3	83.2	+0.1	83.0	81.2	82.8
Mushrooms	88.0	87.3	+0.7	86.8	85.3	86.1
Adult	92.1	92.1	0	92.0	90.6	91.9
Connect 4	88.8	88.6	+0.2	88.4	85.9	88.4
Pumsb-star	86.7	82.2	+4.5	84.1	77.7	81.8
20 NewsGroup	96.0	96.0	0	94.7	90.6	94.7
Voting	99.8	92.4	+7.4	94.8	67.6	64.1
MNIST	93.8	94.5	-0.7	93.0	91.0	92.8
Caltech-101	93.2	94.4	-1.2	92.2	92.0	92.1
Stanford	91.5	91.6	-0.1	69.0	68.4	68.4
SVHN	86.7	91.3	-4.6	92.2	92.0	92.1

AGMs is their generalization capabilities to unseen inference tasks, and experiment II is designed to compare the performance of AGMs against other models when this mismatch occurs.

Concerning data sets, we use: **ten binary data sets** used in previous probabilistic modelling work (example Gens and Pedro [2013]) spanning 16 to 1359 variables, **two binarized image data sets** (28x28 pixels) which are MNIST [LeCun and Cortes, 2010] with digits 0 to 9, and Caltech-101 Silhouettes [Li et al., 2004] with shape outlines from 101 different categories, **one discrete image data set** (30x40 pixels) made of downsampled segmentation masks from the Stanford background dataset, and **one RGB image data set** (32x32 pixels) which is the SVHN dataset with digits of house numbers (see appendix for how we encode continuous RGB values through node marginals).

#### 4.1 Experiment I: Benchmarking

In this experiment, we compare the performance of AGMs against EGMs, on an inference task that the EGMs were specifically optimized for. While we expect EGMs to have slightly superior performance due to this unfair advantage, we observe that AGMs nevertheless show comparable performance.

We calibrate our models on each training data set separately, and test on 1000 unseen points. The inference task `fractional(0.7)` is used to test every model. EGMs train by minimizing the conditional log likelihood score under the inference task given by `fractional(0.5)`. Accuracies are given in table 1 as the percentage of query variables correctly guessed, over all queries formed from the test set. We use identical randomized edge sets of size  $5|\mathcal{V}|$  for non-image data, while a grid graph structure is used with image data (last four rows of table 1).

Results in table 1 show that AGMs trail EGMs on tasks with randomized graphs by a mean EGM-AGM difference of only 2.1, and AGMs surpass EGMs on all image data sets, with a mean EGM-AGM difference of -1.65, despite having never seen these inference tasks during training.

## 4.2 Experiment II: Generalization across inference tasks on images

Experiment I showed that an AGM can be used for inference on `fractional` tasks. In this experiment, we test if an AGM can generalize to other inference tasks, such as `corrupt`, `window` and `quadrant`, despite its inference-agnostic learning style. We also compare against other models which are built for arbitrary conditioning, similar to AGMs. On one hand, we would like to see if an EGM and a VAEAC (described in section 2), both of which assume specific inference tasks during training, generalize to query distributions that they were not exposed to. At the same time, we would like to see how a deep neural architecture like GibbsNet (described in section 2) compares to AGMs, as both of them are trained in an inference-agnostic and adversarial manner. Both VAEAC and GibbsNet follow the architectures given in their original papers.

In this experiment, every candidate model will be *separately* evaluated on `fractional(0.5)`, `window(7)`, `corrupt(0.5)` and `quadrant(1)` tasks. We train *one AGM* and *one GibbsNet architecture*, adversarially, by definition. For EGM and VAEAC, since they assume specific inference tasks during training, we will train:

- *one* EGM and *one* VAEAC by sampling queries successively from *all* inference tasks (MIX scheme)
- *multiple* EGMs and VAEACs, by sampling queries successively from all inference tasks, *except the specific task they are tested on* (MIX-1 scheme).

Tables 2, 3, 4 and 5 show the performances of these models, trained under different schemes (where applicable) and tested on tasks, spread horizontally. The most important metric is indicated in bold, and is the best result, per inference task (per column), obtained by comparing: EGM (MIX-1), VAEAC (MIX-1), GibbsNet and AGM. The MIX-1 scores, when compared to MIX scores, indicate how well EGMs and VAEACs perform on tasks that they have never seen during training. For both VAEACs and EGMs, their performances degrade drastically as soon as they face unseen tasks (seen by the difference between their MIX and MIX-1 rows). This shows that these models do not generalize well to unseen tasks. Out of all the models (EGM (MIX-1), VAEAC (MIX-1), GibbsNet and AGM) whose training procedures were agnostic to the evaluation task of each column in the result tables, AGMs perform the best. AGMs have the highest mean scores (calculated over all inference tasks), for all data sets, out of these models. If a practitioner is confident that their model will *never* have to face unseen inference tasks, then VAEACs may be the best choice for them, given that under the MIX scheme, these models obtain the highest results in most columns.

An interesting observation is that the `corrupt(0.5)` task causes the biggest drop in performances from MIX to MIX-1 schemes for EGMs and VAEACs, and proves to be hard for GibbsNet as well, as the latter learns a latent representation from data, and training data does not have corrupted pixels. AGMs are able to make up for the lack of exposure to corruption through its numerous parameterizations which are specialized to different parts of the data space, compared to the single parameterization of GibbsNet which is bound to be more general. Another interesting result emerges when EGMs are viewed in isolation, and when we compare results obtained on the `fractional(0.5)` task from experiment I to the results obtained on the same task, in experiment II, under the MIX setting. It is clear that preparing discrete undirected graphical models by training them on mixtures of tasks takes away from the specialization obtained when trained on *one* task specifically. Hence, for practitioners who wish to use these models, it is difficult to design a training curriculum that will ensure that the models perform consistently well across tasks. AGMs do not require any extra work

Table 2: Cross-task results on MNIST data. Per column, the bold value is best result between EGM (MIX-1), VAEAC (MIX-1), GibbsNet and AGM, and the shaded result is the best vertically.

<i>Tested on</i>						
<i>Model</i>	<i>Trained on</i>	<b>f=0.5</b>	<b>w=7</b>	<b>c=0.5</b>	<b>q=1</b>	<b>mean</b>
<b>EGM</b>	<b>MIX</b>	93.6 $\pm$ 0.2	66.3 $\pm$ 0.2	82.6 $\pm$ 0.2	86.9 $\pm$ 0.3	82.4
	<b>MIX-1</b>	87.4 $\pm$ 0.1	64.1 $\pm$ 0.3	68.2 $\pm$ 0.1	84.2 $\pm$ 0.1	76.0
<b>VAEAC</b>	<b>MIX</b>	94.2 $\pm$ 0.4	72.4 $\pm$ 0.4	79.8 $\pm$ 0.4	87.9 $\pm$ 0.3	83.6
	<b>MIX-1</b>	85.5 $\pm$ 0.4	61.2 $\pm$ 0.5	65.1 $\pm$ 0.4	81.3 $\pm$ 0.1	73.3
<b>GibbsNet</b>	-	88.6 $\pm$ 0.1	70.5 $\pm$ 0.2	68.0 $\pm$ 0.1	87.1 $\pm$ 0.1	78.6
<b>AGM (Ours)</b>	-	<b>94.5 <math>\pm</math> 0.1</b>	<b>72.3 <math>\pm</math> 0.1</b>	<b>79.2 <math>\pm</math> 0.2</b>	<b>87.4 <math>\pm</math> 0.1</b>	<b>83.4</b>

Table 3: Cross-task results on Caltech-101 data. Per column, the bold value is best result between EGM (MIX-1), VAEAC (MIX-1), GibbsNet and AGM, and the shaded result is the best vertically.

<i>Tested on</i>						
<i>Model</i>	<i>Trained on</i>	<b>f=0.5</b>	<b>w=7</b>	<b>c=0.5</b>	<b>q=1</b>	<b>mean</b>
<b>EGM</b>	<b>MIX</b>	92.0 $\pm$ 0.2	90.0 $\pm$ 0.1	70.2 $\pm$ 0.4	80.6 $\pm$ 0.3	83.2
	<b>MIX-1</b>	81.3 $\pm$ 0.2	88.7 $\pm$ 0.2	55.2 $\pm$ 0.4	79.5 $\pm$ 0.3	76.2
<b>VAEAC</b>	<b>MIX</b>	95.5 $\pm$ 0.5	90.0 $\pm$ 0.5	71.1 $\pm$ 0.4	80.7 $\pm$ 0.5	84.3
	<b>MIX-1</b>	84.2 $\pm$ 0.4	85.6 $\pm$ 0.5	58.4 $\pm$ 0.4	74.9 $\pm$ 0.1	75.8
<b>GibbsNet</b>	-	89.4 $\pm$ 0.1	90.0 $\pm$ 0.3	57.0 $\pm$ 0.4	78.2 $\pm$ 0.1	78.4
<b>AGM (Ours)</b>	-	<b>94.4 <math>\pm</math> 0.3</b>	<b>94.2 <math>\pm</math> 0.3</b>	<b>66.2 <math>\pm</math> 0.5</b>	<b>80.1 <math>\pm</math> 0.1</b>	<b>83.7</b>

Table 4: Cross-task results on Stanford data. Per column, the bold value is best result between EGM (MIX-1), VAEAC (MIX-1), GibbsNet and AGM, and the shaded result is the best vertically.

<i>Tested on</i>						
<i>Model</i>	<i>Trained on</i>	<b>f=0.5</b>	<b>w=7</b>	<b>c=0.5</b>	<b>q=1</b>	<b>mean</b>
<b>EGM</b>	<b>MIX</b>	89.2 $\pm$ 0.5	68.9 $\pm$ 0.4	82.1 $\pm$ 0.5	83.1 $\pm$ 0.5	80.8
	<b>MIX-1</b>	84.1 $\pm$ 0.2	57.8 $\pm$ 0.3	71.8 $\pm$ 0.2	78.3 $\pm$ 0.2	73.0
<b>VAEAC</b>	<b>MIX</b>	89.7 $\pm$ 0.3	76.3 $\pm$ 0.3	82.0 $\pm$ 0.3	83.90 $\pm$ 0.5	83.0
	<b>MIX-1</b>	82.1 $\pm$ 0.3	70.6 $\pm$ 0.5	60.4 $\pm$ 0.4	72.1 $\pm$ 0.2	71.3
<b>GibbsNet</b>	-	87.6 $\pm$ 0.4	<b>75.9 <math>\pm</math> 0.5</b>	61.2 $\pm$ 0.4	78.4 $\pm$ 0.4	75.8
<b>AGM (Ours)</b>	-	<b>91.6 <math>\pm</math> 0.1</b>	75.4 $\pm$ 0.4	<b>80.6 <math>\pm</math> 0.5</b>	<b>82.3 <math>\pm</math> 0.4</b>	<b>82.5</b>

Table 5: Cross-task results on SVHN data. Per column, the bold value is best result between EGM (MIX-1), VAEAC (MIX-1), GibbsNet and AGM, and the shaded result is the best vertically.

<i>Tested on</i>						
<i>Model</i>	<i>Trained on</i>	<b>f=0.5</b>	<b>w=7</b>	<b>c=0.5</b>	<b>q=1</b>	<b>mean</b>
<b>EGM</b>	<b>MIX</b>	91.4 $\pm$ 0.5	81.9 $\pm$ 0.4	74.1 $\pm$ 0.5	91.6 $\pm$ 0.5	84.8
	<b>MIX-1</b>	85.9 $\pm$ 0.5	75.3 $\pm$ 0.3	60.7 $\pm$ 0.4	84.2 $\pm$ 0.4	76.5
<b>VAEAC</b>	<b>MIX</b>	91.8 $\pm$ 0.4	80.0 $\pm$ 0.4	73.1 $\pm$ 0.5	92.5 $\pm$ 0.5	84.4
	<b>MIX-1</b>	88.7 $\pm$ 0.5	64.4 $\pm$ 0.5	70.6 $\pm$ 0.5	87.0 $\pm$ 0.5	77.7
<b>GibbsNet</b>	-	85.1 $\pm$ 0.4	80.2 $\pm$ 0.3	68.0 $\pm$ 0.4	89.1 $\pm$ 0.5	80.6
<b>AGM (Ours)</b>	-	<b>91.3 <math>\pm</math> 0.3</b>	<b>81.4 <math>\pm</math> 0.3</b>	<b>77.8 <math>\pm</math> 0.4</b>	<b>92.4 <math>\pm</math> 0.5</b>	<b>85.7</b>



from practitioners in terms of curriculum design, and AGM performances are close to performances of models which have already been exposed to evaluation tasks.

### 4.3 Experiment III: Sampling using AGMs instead of Gibbs sampling

Motivated by the crisp image samples generated from AGMs and smooth interpolations in latent space (see appendix), we decided to quantify and compare the quality of samples from AGMs, versus from Gibbs samplers defined on EGMs. If one wishes to use a graphical model principally for inference, they would have to make a choice between an EGM and an AGM. In this experiment, we show that AGMs provide added benefits, on top of generalizable inference. Namely, the learner-graphical model pair constitutes a sampler that produces high-quality samples in one shot (one pass from  $z$  to  $\Psi$  to  $x$ ).

We would like some metric for measuring sample quality and we use the following, inspired by previous work on model distillation [Hinton et al., 2015]: given our two samplers, we will use data generated from them, and feed the data to newly-created models for training to solve an inference task, from scratch. The score attained by the new model will indicate the quality of the samples generated by the samplers.

Concretely, we train an AGM (A) and an EGM (B) on some training data set  $D$  from table 1. A is trained adversarially by definition, and B assumes the `fractional(0.5)` inference task. We generate 1000 samples from each model, and call these sampled data sets  $S_1$  and  $S_2$ . If we now train a freshly-created EGM  $E_1$  on  $S_1$  and another one,  $E_2$  on  $S_2$ , from scratch, then test them on the test data set corresponding to  $D$ , then which one out of  $E_1$  or  $E_2$  has better performance, assuming everything else about them is identical? If  $E_1$  performs better, then data from A was of better quality, else, Gibbs sampling on B produced better data. The inference task used to test  $E_1$  or  $E_2$  is `fractional(0.5)`.

For the Gibbs sampler defined on B, we try two scenarios: one where it uses no burn-in cycles to be similar to the one-shot sampling procedure of A, and one scenario where it has 10 burn-in cycles. Interestingly, as seen in table 1, A is better than B regardless of the number of burn-in cycles, bar one exception, and performance when trained on data from A is not that far off the performance from real training data. For B, even 10 burnin steps are not enough for the Markov chain being sampled from to mix. The runtimes of both sampling procedures change linearly with the number of steps used (belief propagation steps with A and Gibbs sampling burnin with B), but since variables have to be sequentially sampled in Gibbs sampling, the process cannot be parallelized across nodes and edges of the graph, yielding poorer runtime, compared to belief propagation which is fully parallelizable and runs entirely through matrix operations on a GPU [Bixler and Huang, 2018] (see appendix for runtime analysis of our method).

In summary, sampling from an AGM is a viable tool and is an added benefit that comes with training AGMs. Our results also indicate that distilling the knowledge from our ensemble into single models may be a promising future line of work.

## 5 Conclusion

The common approach for training undirected graphical models when the test inference task is known a priori, is empirical risk minimization. In this work, we showed that models produced using this approach (EGMs) fail to generalize across tasks. We introduced an adversarial training framework for undirected graphical models, which instead of producing one model, learns an ensemble of parameterizations. The ensemble makes up for mis-specifications in the graphical model structure, and for the approximate nature of belief propagation on graphs of arbitrary topologies. As shown in our experiments, the inference-agnostic nature of our training method allows one AGM to generalize over an array of inference tasks, compared to an EGM which is task-specific. We also compared AGMs against deep neural architectures used for inference with arbitrary conditioning, such as GibbsNet and VAEACs, and AGMs were shown to perform better on unseen inference tasks. Finally, we showed that data can be sampled from AGMs in one shot, presenting an added benefit of using AGMs, and we illustrated that it is possible to distill the knowledge from our ensemble into single models.

## Broader Impact

Graphical models are interpretable models as they expose their independence structures. Such models provide transparency that would allow practitioners to understand biases that may have been imparted to the parameters. If one wishes to understand ways in which a graphical model is biased, one may condition on variables of interest and see exactly how the rest of the variables react.

The fact that our graphical model comes as an ensemble, makes it an editable model. For instance, if the model shows biases towards some characteristic of the data distribution being modeled, one can adapt our approach, and use a weighted recombination [Baruque, 2010] of the individual models in our ensemble, such that the models showing the undesirable bias are suppressed, or they can be completely zeroed out. This is not easy to do in black-box models such as neural networks.

As with most approaches, there are modes of the failure to our model, and the consequences would depend on the setting where the model is used, but the ability to perform arbitrary conditioning with our model can be seen as a safety feature. If our model is used in critical situations where certain combinations of variables have high importance, then our models can be queried with those combinations of variables and their response to such conditions can be well understood and improved, or made safer, if needed.

## Acknowledgments

We gratefully acknowledge support from NSF grant 1723381; from AFOSR grant FA9550-17-1-0165; from ONR grant N00014-18-1-2847; from the Honda Research Institute; from the MIT-IBM Watson AI Lab; and from SUTD Temasek Laboratories. Any opinions, findings, and conclusions or recommendations expressed in this material are those of the authors and do not necessarily reflect the views of our sponsors.

## References

- Waleed Ammar, Chris Dyer, and Noah A. Smith. Conditional random field autoencoders for unsupervised structured prediction. *CoRR*, abs/1411.1147, 2014. URL <http://arxiv.org/abs/1411.1147>.
- Alessandro Antonucci, Giorgio Corani, Denis Deratani Mauá, and Sandra Gabaglio. An ensemble of bayesian networks for multilabel classification. In *Twenty-Third International Joint Conference on Artificial Intelligence*, 2013.
- Dennis Bahler and Laura Navarro. Methods for combining heterogeneous sets of classifiers, 2000.
- B. Baruque. *Fusion Methods for Unsupervised Learning Ensembles*. Studies in Computational Intelligence. Springer Berlin Heidelberg, 2010. ISBN 9783642162046. URL <https://books.google.com/books?id=oVGnmPT0I48C>.
- Peter W. Battaglia, Jessica B. Hamrick, Victor Bapst, Alvaro Sanchez-Gonzalez, Vinícius Flores Zambaldi, Mateusz Malinowski, Andrea Tacchetti, David Raposo, Adam Santoro, Ryan Faulkner, Çağlar Gülçehre, H. Francis Song, Andrew J. Ballard, Justin Gilmer, George E. Dahl, Ashish Vaswani, Kelsey R. Allen, Charles Nash, Victoria Langston, Chris Dyer, Nicolas Heess, Daan Wierstra, Pushmeet Kohli, Matthew Botvinick, Oriol Vinyals, Yujia Li, and Razvan Pascanu. Relational inductive biases, deep learning, and graph networks. *CoRR*, abs/1806.01261, 2018. URL <http://arxiv.org/abs/1806.01261>.
- Mohamed Belghazi, Maxime Oquab, and David Lopez-Paz. Learning about an exponential amount of conditional distributions. In H. Wallach, H. Larochelle, A. Beygelzimer, F. d Alché-Buc, E. Fox, and R. Garnett, editors, *Advances in Neural Information Processing Systems 32*, pages 13703–13714. Curran Associates, Inc., 2019. URL <http://papers.nips.cc/paper/9523-learning-about-an-exponential-amount-of-conditional-distributions.pdf>.
- Luca Bertinetto, João F. Henriques, Jack Valmadre, Philip H. S. Torr, and Andrea Vedaldi. Learning feed-forward one-shot learners. *CoRR*, abs/1606.05233, 2016. URL <http://arxiv.org/abs/1606.05233>.

- Reid Bixler and Bert Huang. Sparse-matrix belief propagation. In *UAI*, 2018.
- Aleksandar Bojchevski, Oleksandr Shchur, Daniel Zügner, and Stephan Günnemann. Netgan: Generating graphs via random walks. In *ICML*, 2018.
- Ramiro Camino, Christian A. Hammerschmidt, and Radu State. Generating multi-categorical samples with generative adversarial networks. *ArXiv*, abs/1807.01202, 2018.
- Liang-Chieh Chen, Alexander G. Schwing, Alan L. Yuille, and Raquel Urtasun. Learning deep structured models. In *Proceedings of the 32nd International Conference on International Conference on Machine Learning - Volume 37*, ICML’15, page 1785–1794. JMLR.org, 2015.
- Edward Choi, Siddharth Biswal, Bradley Malin, Jon Duke, Walter F. Stewart, and Jimeng Sun. Generating multi-label discrete patient records using generative adversarial networks. In *MLHC*, 2017.
- LI Chongxuan, Max Welling, Jun Zhu, and Bo Zhang. Graphical generative adversarial networks. In *Advances in neural information processing systems*, pages 6069–6080, 2018.
- J. Domke. Learning graphical model parameters with approximate marginal inference. *IEEE Transactions on Pattern Analysis and Machine Intelligence*, 35(10):2454–2467, 2013.
- Justin Domke. Implicit differentiation by perturbation. In J. D. Lafferty, C. K. I. Williams, J. Shawe-Taylor, R. S. Zemel, and A. Culotta, editors, *Advances in Neural Information Processing Systems 23*, pages 523–531. Curran Associates, Inc., 2010. URL <http://papers.nips.cc/paper/4107-implicit-differentiation-by-perturbation.pdf>.
- Jeff Donahue, Philipp Krähenbühl, and Trevor Darrell. Adversarial feature learning. *CoRR*, abs/1605.09782, 2016. URL <http://arxiv.org/abs/1605.09782>.
- Hao-Wen Dong and Yi-Hsuan Yang. Training generative adversarial networks with binary neurons by end-to-end backpropagation. *CoRR*, abs/1810.04714, 2018. URL <http://arxiv.org/abs/1810.04714>.
- Laura Douglas, Iliyan Zarov, Konstantinos Gourgoulis, Chris Lucas, Chris Hart, Adam Baker, Maneesh Sahani, Yura Perov, and Saurabh Johri. A universal marginalizer for amortized inference in generative models. *CoRR*, abs/1711.00695, 2017. URL <http://arxiv.org/abs/1711.00695>.
- Vincent Dumoulin, Ishmael Belghazi, Ben Poole, Alex Lamb, Martín Arjovsky, Olivier Mastropietro, and Aaron C. Courville. Adversarially learned inference. *ArXiv*, abs/1606.00704, 2017.
- Rizal Fathony and Naveen Goela. Discrete wasserstein generative adversarial networks (dwgan). 2018.
- Rizal Fathony, Ashkan Rezaei, Mohammad Ali Bashiri, Xinhua Zhang, and Brian Ziebart. Distributionally robust graphical models. In S. Bengio, H. Wallach, H. Larochelle, K. Grauman, N. Cesa-Bianchi, and R. Garnett, editors, *Advances in Neural Information Processing Systems 31*, pages 8344–8355. Curran Associates, Inc., 2018. URL <http://papers.nips.cc/paper/8055-distributionally-robust-graphical-models.pdf>.
- Yoav Freund and Robert Schapire. A short introduction to boosting. *Journal-Japanese Society For Artificial Intelligence*, 14(771-780):1612, 1999.
- G. Fumera and F. Roli. A theoretical and experimental analysis of linear combiners for multiple classifier systems. *IEEE Transactions on Pattern Analysis and Machine Intelligence*, 27(6): 942–956, 2005.
- Robert Gens and Domingos Pedro. Learning the structure of sum-product networks. In Sanjoy Dasgupta and David McAllester, editors, *Proceedings of the 30th International Conference on Machine Learning*, volume 28 of *Proceedings of Machine Learning Research*, pages 873–880, Atlanta, Georgia, USA, 17–19 Jun 2013. PMLR. URL <http://proceedings.mlr.press/v28/gens13.html>.

- Justin Gilmer, Samuel S. Schoenholz, Patrick F. Riley, Oriol Vinyals, and George E. Dahl. Neural message passing for quantum chemistry. *CoRR*, abs/1704.01212, 2017. URL <http://arxiv.org/abs/1704.01212>.
- Ian J. Goodfellow, Jean Pouget-Abadie, Mehdi Mirza, Bing Xu, David Warde-Farley, Sherjil Ozair, Aaron C. Courville, and Yoshua Bengio. Generative adversarial networks. *ArXiv*, abs/1406.2661, 2014.
- Ishaan Gulrajani, Faruk Ahmed, Martín Arjovsky, Vincent Dumoulin, and Aaron C. Courville. Improved training of wasserstein gans. *ArXiv*, abs/1704.00028, 2017.
- Geoffrey Hinton, Oriol Vinyals, and Jeff Dean. Distilling the knowledge in a neural network, 2015.
- R. Devon Hjelm, Athul Paul Jacob, Tong Che, Kyunghyun Cho, and Yoshua Bengio. Boundary-seeking generative adversarial networks. *ArXiv*, abs/1702.08431, 2017.
- Dirk Husmeier and J. G. Taylor. *Neural Networks for Conditional Probability Estimation: Forecasting beyond Point Predictions*. Springer-Verlag, Berlin, Heidelberg, 1st edition, 1999. ISBN 1852330953.
- Oleg Ivanov, Michael Figurnov, and Dmitry Vetrov. Variational autoencoder with arbitrary conditioning, 2019.
- Robert A Jacobs, Michael I Jordan, Steven J Nowlan, and Geoffrey E Hinton. Adaptive mixtures of local experts. *Neural computation*, 3(1):79–87, 1991.
- Eric Jang, Shixiang Gu, and Ben Poole. Categorical reparameterization with gumbel-softmax. *ArXiv*, abs/1611.01144, 2017.
- Matthew J. Johnson, David Duvenaud, Alexander B. Wiltschko, Ryan P. Adams, and Sandeep Robert Datta. Composing graphical models with neural networks for structured representations and fast inference. In *NIPS*, 2016.
- Theofanis Karaletsos. Adversarial message passing for graphical models. *ArXiv*, abs/1612.05048, 2016.
- Daphne Koller and Nir Friedman. *Probabilistic Graphical Models: Principles and Techniques - Adaptive Computation and Machine Learning*. The MIT Press, 2009. ISBN 0262013193.
- Volodymyr Kuleshov and Stefano Ermon. Neural variational inference and learning in undirected graphical models. *CoRR*, abs/1711.02679, 2017. URL <http://arxiv.org/abs/1711.02679>.
- Alex Kulesza and Fernando Pereira. Structured learning with approximate inference. In *Advances in Neural Information Processing Systems 20*. Cambridge, MA, 2008. URL [http://books.nips.cc/papers/files/nips20/NIPS2007\\_0809.pdf](http://books.nips.cc/papers/files/nips20/NIPS2007_0809.pdf).
- Alex Lamb, R. Devon Hjelm, Yaroslav Ganin, Joseph Paul Cohen, Aaron C. Courville, and Yoshua Bengio. Gibbsnet: Iterative adversarial inference for deep graphical models. In *NIPS*, 2017.
- Yann LeCun and Corinna Cortes. MNIST handwritten digit database. 2010. URL <http://yann.lecun.com/exdb/mnist/>.
- Fei-Fei Li, Rob Fergus, and Pietro Perona. Learning generative visual models from few training examples: An incremental bayesian approach tested on 101 object categories. *2004 Conference on Computer Vision and Pattern Recognition Workshop*, pages 178–178, 2004.
- Ye-Hua Liu and David Poulin. Neural belief-propagation decoders for quantum error-correcting codes. *Physical review letters*, 122 20:200501, 2019.
- Mehdi Mirza and Simon Osindero. Conditional generative adversarial nets. *CoRR*, abs/1411.1784, 2014. URL <http://arxiv.org/abs/1411.1784>.
- Tsendsuren Munkhdalai and Hong Yu. Meta networks. *CoRR*, abs/1703.00837, 2017. URL <http://arxiv.org/abs/1703.00837>.

- Kevin Murphy, Yair Weiss, and Michael I. Jordan. Loopy belief propagation for approximate inference: An empirical study, 2013.
- Kevin P. Murphy. *Machine Learning: A Probabilistic Perspective*. The MIT Press, 2012. ISBN 0262018020.
- Meng Qu, Yoshua Bengio, and Jian Tang. Gmnn: Graph markov neural networks. In *ICML*, 2019.
- Victor Garcia Satorras and M. Welling. Neural enhanced belief propagation on factor graphs. *ArXiv*, abs/2003.01998, 2020.
- Victor Garcia Satorras, Zeynep Akata, and M. Welling. Combining generative and discriminative models for hybrid inference. *ArXiv*, abs/1906.02547, 2019.
- Haozhen Situ, Zhi-Min He, Lvzhou Li, and Shenggen Zheng. Quantum generative adversarial network for generating discrete data. 2018.
- Veselin Stoyanov, Alexander Ropson, and Jason Eisner. Empirical risk minimization of graphical model parameters given approximate inference, decoding, and model structure. In Geoffrey Gordon, David Dunson, and Miroslav Dudík, editors, *Proceedings of the Fourteenth International Conference on Artificial Intelligence and Statistics*, volume 15 of *Proceedings of Machine Learning Research*, pages 725–733, Fort Lauderdale, FL, USA, 11–13 Apr 2011. PMLR. URL <http://proceedings.mlr.press/v15/stoyanov11a.html>.
- Jonathan Tompson, Arjun Jain, Yann LeCun, and Christoph Bregler. Joint training of a convolutional network and a graphical model for human pose estimation. *CoRR*, abs/1406.2984, 2014. URL <http://arxiv.org/abs/1406.2984>.
- Lifu Tu and Kevin Gimpel. Learning approximate inference networks for structured prediction. *CoRR*, abs/1803.03376, 2018. URL <http://arxiv.org/abs/1803.03376>.
- Martin Wainwright, Tommi Jaakkola, and Alan Willsky. Tree-reweighted belief propagation algorithms and approximate ml estimation by pseudo-moment matching. 21, 12 2002.
- Hongwei Wang, Jia Wang, Jialin Wang, Miao Zhao, Weinan Zhang, Fuzheng Zhang, Xing Xie, and Minyi Guo. Graphgan: Graph representation learning with generative adversarial nets. *CoRR*, abs/1711.08267, 2017. URL <http://arxiv.org/abs/1711.08267>.
- Lei Xu, Maria Skoularidou, Alfredo Cuesta-Infante, and Kalyan Veeramachaneni. Modeling tabular data using conditional GAN. *CoRR*, abs/1907.00503, 2019. URL <http://arxiv.org/abs/1907.00503>.
- KiJung Yoon, Renjie Liao, Yuwen Xiong, Lisa Zhang, Ethan Fetaya, Raquel Urtasun, Richard S. Zemel, and Xaq Pitkow. Inference in probabilistic graphical models by graph neural networks. *CoRR*, abs/1803.07710, 2018. URL <http://arxiv.org/abs/1803.07710>.
- Zhen Zhang, Fan Wu, and Wee Sun Lee. Factor graph neural network. *CoRR*, abs/1906.00554, 2019. URL <http://arxiv.org/abs/1906.00554>.
- Shuai Zheng, Sadeep Jayasumana, Bernardino Romera-Paredes, Vibhav Vineet, Zhizhong Su, Dalong Du, Chang Huang, and Philip H. S. Torr. Conditional random fields as recurrent neural networks. *CoRR*, abs/1502.03240, 2015. URL <http://arxiv.org/abs/1502.03240>.
- Zilong Zhong and Jonathan Li. Generative adversarial networks and probabilistic graph models for hyperspectral image classification. *CoRR*, abs/1802.03495, 2018. URL <http://arxiv.org/abs/1802.03495>.

## 6 Appendix

In this section, we present additional information concerning our experiments.

- Section 6.1 presents details about model architectures and hyperparameters.
- Section 6.2 describes how we use our discrete undirected probabilistic graphical models to model continuous RGB values in the case of the SVHN dataset.
- Section 6.3 provides an analysis of the time and memory complexities of our method.
- Section 6.4 provides empirical evidence of how accuracies obtained by our inference machine change with the sizes of ensembles used, under the setup of experiment I.
- Section 6.5 displays unconditional samples from AGMs.

### 6.1 Experiment details common to all experiments

All our experiments are run using PyTorch for automatic differentiation, on a Volta V100 GPU.

#### Architectures:

All architectures are feed forward, consisting of linear layers, with or without Batch Normalization, and with or without Dropout. Activation functions for linear layers are LeakyRelu, Sigmoid or none.

- The **EGM** method has no neural module, all the parameters (edge potentials) are real numbers contained in matrices, with belief propagation implemented entirely through matrix operations (with no iteration over edges).
- For the **AGM**, there are two neural modules:
  1. Learner  $L_\theta : \mathbb{R}^m \rightarrow \mathbb{R}^{|E||\mathcal{X}|^2}$  converting  $z$  to potentials  $\Psi$ :  
*Linear(in= $m$ , out= $2m$ ); Batch Normalization; Leaky ReLU (neg slope 0.1)*  
*Linear(in= $2m$ , out= $|E||\mathcal{X}|^2$ )*
  2. Discriminator  $D_w : \mathbb{R}^{N|\mathcal{X}|} \rightarrow \mathbb{R}$  converting data  $x$  to Wasserstein-1 distance:  
*Linear(in= $N|\mathcal{X}|$ , out= $2N|\mathcal{X}|$ ); Dropout(0.2); Leaky ReLU (neg slope 0.1)*  
*Linear(in= $2N|\mathcal{X}|$ , out= $2N|\mathcal{X}|$ ); Dropout(0.2); Leaky ReLU (neg slope 0.1)*  
*Linear(in= $2N|\mathcal{X}|$ , out=1); Dropout(0.2)*
- GibbsNet and VAEAC architectures follow from the original papers describing these models.

#### Note about data $(x)$ being in $\mathbb{R}^{N|\mathcal{X}|}$ :

Instead of using categorical samples as our generated data (obtained from marginal probability distributions  $\mu_i$ , produced for every variable), we follow the WGAN-GP method where the generated data is a *concatenation* of the marginals in some specific order. This implies that true samples from the train data set also have to be processed into a concatenation of the  $\mathcal{X}$ -dimensional one-hot encodings of the values they propose for every node, to meet the input specifications of the discriminator. This method for discrete GANs is used both for AGMs and GibbsNet in our implementation.

#### Hyperparameters:

- $z$  is sampled from standard multivariate Gaussian  $\mathcal{N}(0, I_m)$ , and the dimensionality  $m$  was picked depending on  $N$ , the number of random variables involved in the data. When  $N$  is smaller than 500, we use  $m = 64$  and otherwise,  $m = 128$  is used.
- For the ensemble, we used  $M = 1000$ , where  $M$  is the number of models used for the pooling mechanism.
- In both the EGM and AGM, we need to carry out belief propagation. The number of steps of belief propagation was kept constant and was 25 in EGM, 5 in AGM. These numbers gave the best results for their respective models.
- For the AGM method,  $\lambda = 10$  was used for the coefficient of the regularization term of equation.
- Also, our implementation of the WGAN-GP method for adversarial training, the discriminator is trained for 10 steps, for every update step on the generator.
- The learning rates are  $1e - 2$  for EGM (matrix of parameters) and  $1e - 4$  for the AGM (learner and discriminator).

- We used 500 and 3000 training gradient descent steps enough across data sets to train the EGMs and AGMs respectively.
- The batch sizes used were 128 for training both AGM and EGM, and for testing the AGM, with  $M = 1000$ , the batch sizes used were reduced to 16.
- The Adam optimizer was used for all models across experiments.

## 6.2 Note on modelling continuous RGB variables

For the SVHN data set, we encode continuous RGB values in the range  $[0, 1]$  through bernoulli probability distributions (discrete support is  $\{0, 1\}$ ) at every node. For example, to encode an observed pixel value of 0.2, we would assign a prior probability of 0.2 to the event where that node takes on value 1, and a prior probability of  $1 - 0.2 = 0.8$  to the event where that node takes on value 0. After belief propagation, we decode values from every node to be the probability mass assigned to the value 1, which is equivalent to the expected value from the node marginal probability distribution, since it is a bernoulli distribution. The rest of our method stays the same.

## 6.3 Computational complexity

In this section, we summarize the computational complexity of our approach. The  $\text{inference}(x_{\mathcal{E}}, \Psi, t)$  procedure is used throughout our work. Given a graphical model structure (with edge set  $E$ , node set  $V$  and discrete support  $\mathcal{X}$ ), one parameter vector  $\Psi$  and observations  $x_{\mathcal{E}}$ , it performs  $t$  steps of belief propagation to produce node-wise approximate marginal probability distributions conditioned on  $x_{\mathcal{E}}$ . Assuming that one pass through our neural learner and discriminator take constant time, this inference process is the bottleneck in our approach.

### 6.3.1 Time complexity

From the highest layer of abstraction, if we assume the time complexity of the  $\text{inference}$  procedure to be  $\mathcal{O}(f(|E|, |V|, |\mathcal{X}|, t))$ , then our training procedure has time complexity  $\mathcal{O}(Nf(|E|, |V|, |\mathcal{X}|, t))$  where  $N$  is the number of fake data points that we generate and feed to the discriminator, by calling the  $\text{inference}$  procedure  $N$  times with  $\mathcal{E} = \emptyset$ .

During the inference phase, we carry out  $M$  calls to the  $\text{inference}$  procedure (with  $\mathcal{E} \neq \emptyset$ ) to get  $M$  different conditional node-wise marginal probability distributions for every query. If the number of inference queries to be attended to is  $Q$ , then the inference phase has time complexity  $\mathcal{O}(MQf(|E|, |V|, |\mathcal{X}|, t))$ .

Our implementation of belief propagation follows that of [Bixler and Huang, 2018], where the process is fully parallelized over nodes and edges and run on a GPU with  $k$  cores. The time complexity of running belief propagation for  $t$  iterations *without* any parallelization, is  $\mathcal{O}(t|E||\mathcal{X}|^2)$  and in their implementation, the time complexity is improved to  $\mathcal{O}(t \lceil \frac{|E|}{k} \rceil |\mathcal{X}||\sigma| + \lceil t \frac{|E||\mathcal{X}|^2}{k} \rceil)$ , where  $\sigma$  is the maximum neighborhood size across the graph. We refer the interested reader to their work for a detailed derivation of this result, which implies that the time complexity of running inference through our ensemble to answer a batch of  $Q$  queries is  $\mathcal{O}(MQt \lceil \frac{|E|}{k} \rceil |\mathcal{X}||\sigma| + MQt \lceil \frac{|E||\mathcal{X}|^2}{k} \rceil)$ .

### 6.3.2 Space complexity

To achieve fully-matricized belief propagation, the largest matrices kept in memory during the process are two  $|E| \times |E|$  matrices. While these are typically sparse matrices, in the worst case, the memory demand for belief propagation has asymptotic complexity  $\mathcal{O}(|E|^2)$ . During our training procedure, when generating data from a batch of  $B$  different random vectors, the memory demand scales with complexity  $\mathcal{O}(B|E|^2)$ , and during inference, with  $M$  parallel calls to the  $\text{inference}$  procedure to resolve a batch of  $Q$  queries, the memory demand scales as  $\mathcal{O}(QM|E|^2)$ .

## 6.4 Ensemble size considerations

We benchmark the performance of the AGM model only, with varying ensemble sizes  $M$ . Essentially, we follow the exact same setup as experiment I for the AGM, except that during inference, we will

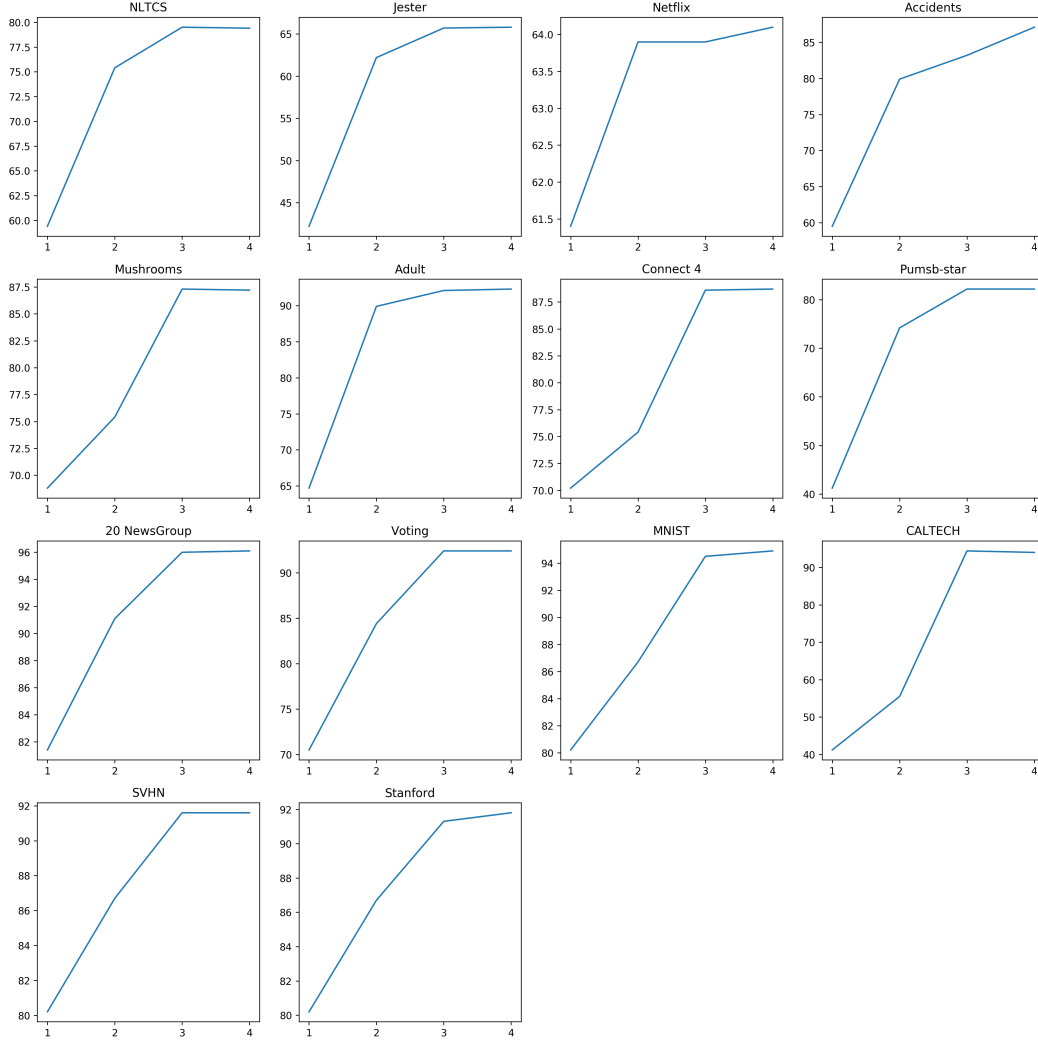


Figure 3: Inference accuracies (vertical axes) obtained across datasets, using the AGM model (experiment I), where the variable being varied in every plot is the ensemble size  $M$  (horizontal axes) used during inference. Values used for  $M$  were 10, 100, 1000, 10000, indicated in logarithm base 10.

separately try values of  $M = 10, 100, 1000, 10000$  in an attempt to understand what size of ensemble would give the best results. Results are summarized in the plots of figure 3.

At the lowest ensemble size of  $M = 10$ , performances are much lower than the best performances, showing that only 10 models are not enough to form a solid opinion and with such a small population size, the models may even be strongly favoring bad choices (lower than chance performance). The largest increases in performance were from  $M = 10$  to  $M = 100$ , showing that already at  $M = 100$ , the ensemble effect is positive. The best performances are reached in almost every data set at  $M = 1000$ , barring some exceptions. The increase in performance, from  $M = 100$  to  $M = 1000$ , though, is smaller than the increase from  $M = 10$  to  $M = 100$ . From  $M = 1000$  to  $M = 10000$  however, there is practically no increase in performance, and in terms of memory, we are unable to fully parallelize the inference procedure across 10000 models on 1 GPU, forcing us to break the process into several serial steps.  $M = 1000$  is the best ensemble size when both performance and practicality are considered.



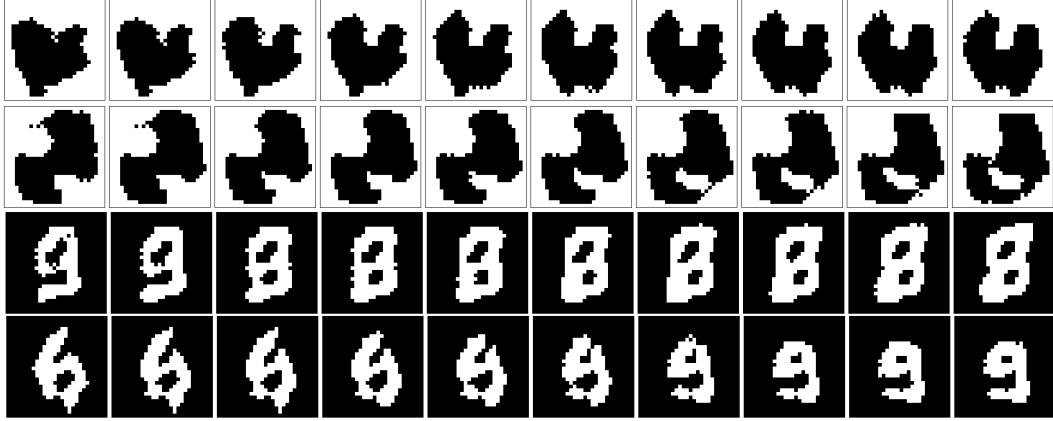


Figure 4: Images (column 1) generated from the AGM by providing different random latent vectors  $z$  to AGM trained on MNIST (rows 1-2) and Caltech-101 (rows 3-4). Horizontally across every row, the random vectors are gradually changed to a target latent vector. Images are crisp and transition smoothly from source to target.

### 6.5 The AGM as viewed as a GAN generator

When fed random  $z$  vectors, our AGM produces samples which look crisp when the data being learned on is pictorial, and we also see smooth interpolations in latent space. This is an interesting result in the space of discrete GANs, given that CNNs were not included in the architecture. We show samples generated by our AGM when trained on MNIST data in figure 4.